

Anomalous giant piezoresistance in AlAs 2D electrons with anti-dot lattices

O. Gunawan, T. Gokmen, Y. P. Shkolnikov, E. P. De Poortere, and M. Shayegan
Department of Electrical Engineering, Princeton University, Princeton, NJ 08544

(Dated: September 15, 2021)

An AlAs two-dimensional electron system patterned with an anti-dot lattice exhibits a giant piezoresistance (GPR) effect, with a sign opposite to the piezoresistance observed in the unpatterned region. We trace the origin of this anomalous GPR to the non-uniform strain in the anti-dot lattice and the exclusion of electrons occupying the two conduction band valleys from different regions of the sample. This is analogous to the well-known giant magnetoresistance (GMR) effect, with valley playing the role of spin and strain the role of magnetic field.

PACS numbers: 72.20.-i, 73.23.Ad, 75.47.Jn

Currently there is considerable interest in electronic devices whose operating principles go beyond the conventional, charge-based electronics. A prime example is the giant magnetoresistance (GMR) device [1], one of the first members of a new class of "spintronic" devices [2, 3] whose operation rests on the manipulation of electron's spin degree of freedom. In certain solids the electrons can reside in multiple conduction band minima (or valleys) and therefore have yet another, *valley*, degree of freedom. Here we report a giant, low temperature piezoresistance (GPR) effect in a two-valley AlAs two-dimensional electron system (2DES) patterned with anti-dot lattices. The effect is among the strongest seen in any system and allows the detection of minute strains and displacements via a simple resistance measurement. And yet it is anomalous as it has the opposite sign compared to the conventional piezoresistance found in multi-valley semiconductors [4, 5]. Using magnetoresistance measurements and numerical simulations, we propose a model that qualitatively explains the observed GPR effect based on the non-uniform strain and the exclusion of electrons occupying the two conduction band valleys from different regions of the sample. This is analogous to the operating principle of the GMR effect: here valley plays the role of spin and strain the role of magnetic field. These results highlight the fundamental analogy between the spin and valley degrees of freedom [6, 7] and point to new opportunities in developing novel "valleytronic" devices whose functionality relies on the control and manipulation of the electron's valley degree of freedom [8, 9].

We performed experiments on a 2DES in a modulation doped, 11 nm-wide AlAs quantum well. In this system the electrons occupy two in-plane, anisotropic conduction band valleys with elliptical Fermi contours [10], characterized by a heavy longitudinal mass $m_l = 1.1m_0$ and light transverse mass $m_t = 0.2m_0$, where m_0 is electron mass in vacuum. We label these as X and Y valleys, according to the direction of their major axes, [100] and [010], as shown in the lower inset of Fig. 1 [11]. We patterned a Hall bar along the [100] direction using standard photo lithography technique. Then, via electron beam lithography and dry etching using an electron cyclotron

resonance etcher we defined three anti-dot (AD) lattices with periods $a = 1, 0.8$ and $0.6 \mu\text{m}$ in three regions of the Hall bar, and left a fourth region un-patterned (blank) [see the upper insets of Fig. 1]. Each AD lattice is an array of holes (ADs) etched to a depth of $\simeq 300$ nm into the sample thus depleting the 2DES in the hole area (the 2DES is at a depth of $\simeq 100$ nm from the top surface). The ratio d/a for each AD cell is $\sim 1:3$, where d is the AD diameter. We also deposited Ti/Au back- and front-gates to control the total 2DES density (n) in the sample. To apply tunable strain, we glued the sample to one side of a piezo-actuator [12], and monitored the applied strain using a metal-foil strain-gauge glued to the piezo's other side. We define strain as $\epsilon = \epsilon_{[100]} - \epsilon_{[010]}$ where $\epsilon_{[100]}$ and $\epsilon_{[010]}$ are the fractional length changes of the sample along the [100] and [010] directions, respectively. Note that for $\epsilon > 0$ electrons are transferred from the X valley to the Y valley while n stays constant [11]. Further fabrication details and characteristics of the blank region of the particular sample used in this study were reported in Ref. [6]. In particular, at a piezo bias (V_P) of -250 V, the X and Y valleys in the blank region are equally occupied (balanced) and, at $n = 3.8 \times 10^{11} / \text{cm}^2$ where the data of Fig. 1 were taken, electrons are all transferred to the Y valley for $V_P > 50$ V ($\epsilon > 1.5 \times 10^{-4}$); see the lower insets in Fig. 1. The measurements were performed in a ^3He cryostat with a base temperature of 0.3 K.

The lower trace in Fig. 1 shows the piezoresistance (PR) in the blank region. The PR exhibits the anticipated behavior: the resistance drops with increasing strain as the electrons are transferred to the Y valley whose mobility is higher (because of its smaller effective mass, m_t) along the current direction. Beyond the valley depopulation point ($\epsilon > 1.5 \times 10^{-4}$), the resistance starts to saturate at a low value as the intervalley electron transfer ceases. This is the conventional PR effect in AlAs 2DES as has been reported in Ref. [5]. The dotted line in Fig. 1 represents the best fit of the data to a simple model [5], which assumes that the valley populations change linearly with strain, and adds the conductivities of the two valleys to find the total conductivity; the model also assumes an isotropic scattering time for

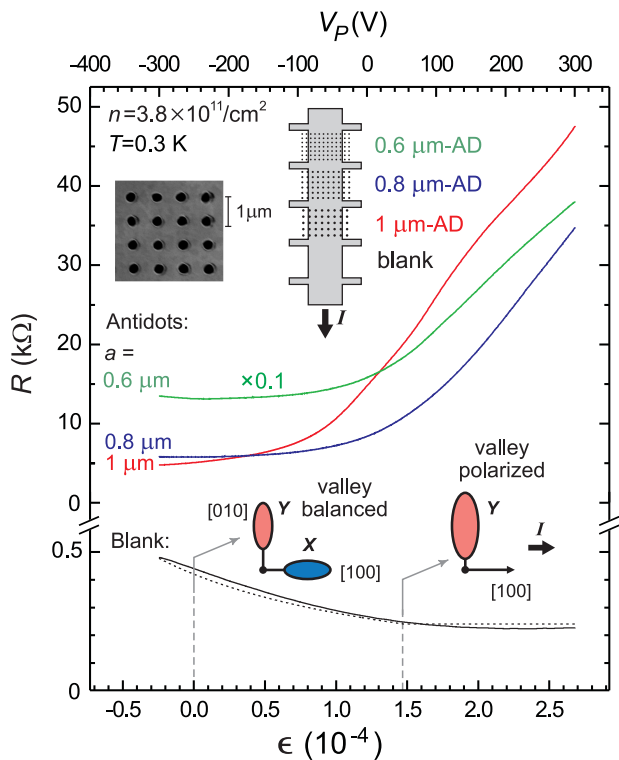


FIG. 1: (Color online) The piezoresistance of an AlAs 2DES in the un-patterned (blank) region (lower trace) and in three anti-dot (AD) regions (upper three traces). The dotted line is the best fit to the piezoresistance in the blank region based on a conventional model. Upper insets: A micrograph of an AD lattice ($a=0.8 \mu\text{m}$) and sections of the Hall bar. Lower insets: The orientation and occupation of the valleys are schematically shown for the blank region at $\epsilon = 0$ where the two valleys are equally occupied and for $\epsilon > 1.5 \times 10^{-4}$ where all the electrons are transferred to the Y valley.

both valleys and ignores the inter-valley scattering.

The upper three traces in Fig. 1 represent the PR of the AD regions and demonstrate our main finding. These traces exhibit an *increasing* resistance as a function of strain, opposite to the PR in the blank region. The strength of the PR effect is also quite prominent in the AD regions: indeed, in the $1 \mu\text{m}$ -AD region the resistance changes by about ten times for the range of applied strain while, in contrast, the change for the blank region is only about a factor of two. Furthermore, for all three AD regions, the PR persists beyond the valley depopulation point of the blank region ($\epsilon > 1.5 \times 10^{-4}$) where the blank region's PR nearly saturates.

These observations highlight the remarkable difference between the PR effect in the blank and the AD regions and present an interesting puzzle. As we will now show, it is the presence of the AD lattice, which significantly modifies the strain distribution in the AlAs 2DES, that leads to the anomalous PR. To understand the strain distribution in the AD regions we performed a simple

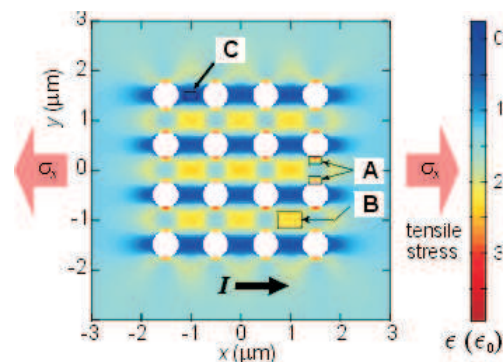


FIG. 2: (Color online) Finite element simulation of the strain distribution in a 2D medium perforated with an AD lattice. Boxes A and B highlight the areas of enhanced strain, while box C highlights a region of reduced strain.

finite-element-method simulation (using FEMLAB) for a plane-strain problem of a 2D medium perforated with an array of holes. We apply a small tensile stress σ_x to the left and right sides, producing a small amount of strain ϵ_0 at $(x, y) \rightarrow \pm\infty$; in other words, if there were no AD lattice, the strain would be uniform everywhere with a magnitude equal to ϵ_0 . The result of this simulation is shown in Fig. 2. There is clearly a non-uniform strain distribution due to the presence of the AD lattice. In particular, there are localized regions of enhanced strain (boxes A and B in Fig. 2), and of essentially zero strain (box C). For example, in the upper and lower periphery of the AD (box A) the strain is enhanced by as much as $3\epsilon_0$. This enhancement by $3\epsilon_0$ is indeed indicated by an analytical solution of a 2D plane strain problem with a single hole [13]. We add that our simulation of Fig. 2 is for a 2D system, however, we expect that in a system which contains an AD lattice at its top surface, the strain profile is qualitatively similar to what is shown in Fig. 2.

But how does a non-uniform strain distribution lead to an increase in resistance? Note that, in our experiment, positive (negative) strain leads to a valley splitting that favors the Y valley (X valley) occupation. This means that electrons occupying either the X or Y valley feel an extra, modulated, and confining potential (besides being excluded from the AD hole regions) as they move through the AD lattice. We believe that it is this potential that profoundly affects the quasi-ballistic motion of electrons in the AD region and leads to the observed PR. For example, consider the localized enhancement of positive strain in box A of Fig. 2. Such strain depletes the X-valley electrons in box A and effectively narrows the width of the channels (between the holes) through which they have to travel to carry current to the right. In the remainder of the paper we present evidence from additional measurements and numerical simulations that lend further support to this picture.

In Fig. 3(a) we show resistance vs. perpendicular mag-

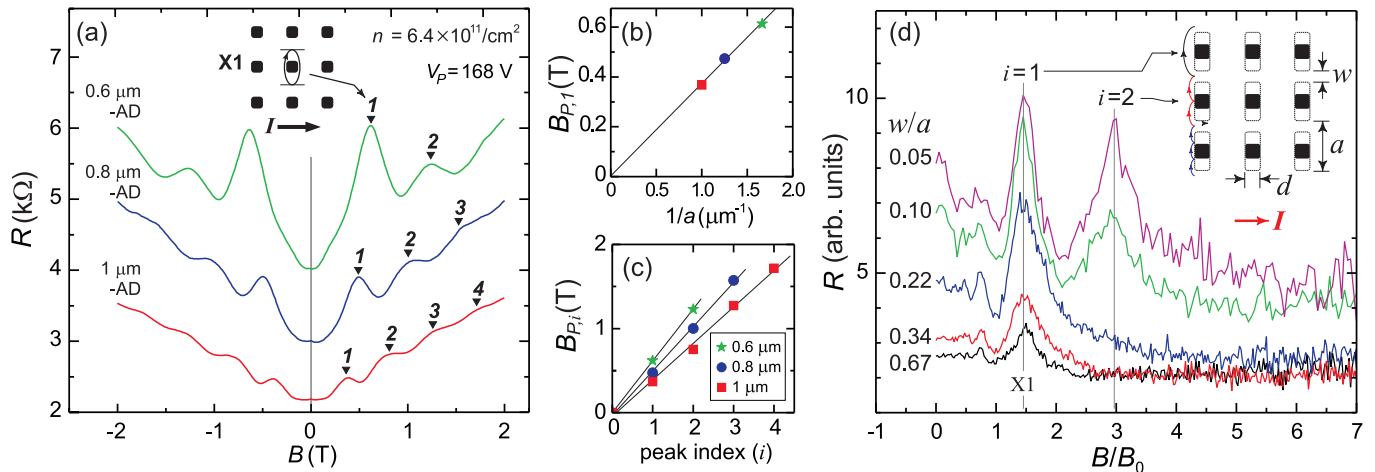


FIG. 3: (Color online) (a) Magnetoresistance of the AD regions showing the commensurability peaks labeled with indices $i = 1, 2, \dots$. Inset: X1 orbit associated with the fundamental ($i = 1$) peak. (b) The $i = 1$ peak position $B_{P,1}$ vs. reciprocal AD lattice spacing $1/a$. (c) Peak positions $B_{P,i}$ vs. index i . Each set of data points fits well to a straight line that goes through the origin. (d) Numerical simulations of the X -valley electron transport through ADs with variable channel width. B_0 is the magnetic field of the first commensurate orbit (X1) if the Fermi contour were circular. Inset: Schematic diagram of the elongated AD lattice with channel width w and period a , and the bouncing orbits that give rise to sub-harmonic peaks. The black areas are the original AD (holes), the lines mark the boundaries of the hypothesized, local strain-induced, "extended AD".

netic field (B) traces for the three AD regions, taken at $V_P = 168$ V ($\epsilon = 2 \times 10^{-4}$). Each trace exhibits a series of peaks that we label with indices $i = 1, 2, 3, \dots$. These peaks are associated with the geometric resonance, or the commensurability, of the cyclotron orbits and the AD lattice period. Such commensurate orbits are well-known to occur in 2DESs with AD lattices [14, 15], although, as we discuss below, the presence of the $i > 1$ peaks is unusual. If we plot the positions of the peaks ($B_{P,i}$) vs. their indices as shown in Fig. 3(c), we observe that $B_{P,i}$ scales linearly with i for all AD regions. We refer to the $i = 1$ peak as the fundamental peak and $i = 2, 3, \dots$ peaks as the subharmonic peaks. First we focus our analysis of the fundamental peak and then present a detailed analysis of the subharmonic peaks.

Figure 3(b) presents a plot of the fundamental peak positions $B_{P,1}$ vs. the reciprocal AD lattice spacing $1/a$. The observed linear dependence is consistent with the geometric scaling of the peak positions as expected from the relationship: $B_P = \hbar k_F / ea$, where k_F is the Fermi wave vector of the commensurate orbit in the direction perpendicular to the current flow [15]. In fact, in Ref. [15], systematic measurements and analysis of $B_{P,1}$ as a function of n and a were made in an AlAs 2DES with AD lattices but without any applied strain. Both experimental data and simulations showed that, while the two valleys X and Y could in principle give rise to two sets of commensurate orbits, it is the X1 orbit [Fig. 3(a) inset] that gives rise to the fundamental magnetoresistance peak. The data in Fig. 3 are consistent with this finding: If we assign the fundamental peak to the Y1 orbit (simi-

lar to X1 except rotated by 90°), we find that the corresponding Y -valley densities deduced from the positions of these peaks are unphysically large (greater than the total electron density, n , determined from the Shubnikov de-Haas oscillations). We have repeated such analysis at various n and ϵ , and have reached a similar conclusion. Therefore, we surmise that the fundamental peak $B_{P,1}$ is associated with the X1 orbit.

Now we focus on the sub-harmonic magnetoresistance peaks ($i > 1$) observed in Fig. 3(a). Such peaks are *not* observed in the absence of strain, e.g., in the experiments of Ref. [15], and their presence in Fig. 3(a) traces in fact provides clues for the shape of the potential seen by the X -valley electrons in the present sample. While subharmonic peaks are seldom seen in AD lattices, they are readily observed in transverse magnetic focusing (TMF) experiments [16, 17] where ballistic electrons are emitted through a narrow opening and are collected at a second narrow opening which is at a relatively large distance away. Under such conditions, the injected ballistic electrons can bounce off the TMF barrier one or more times as they follow their cyclotron orbit trajectories, and magnetoresistance peaks are observed whenever the emitter-collector distance equals a multiple integer of the orbit diameter (an illustration of this is shown in Fig. 3(d) inset for our structure.) We emphasize that in TMF structures, the distance between the emitter and collector is typically larger than the width of the emitter and collector openings thus allowing bouncing trajectories to occur. Furthermore, the narrow openings also produce better focusing and therefore sharp subharmonic peaks.

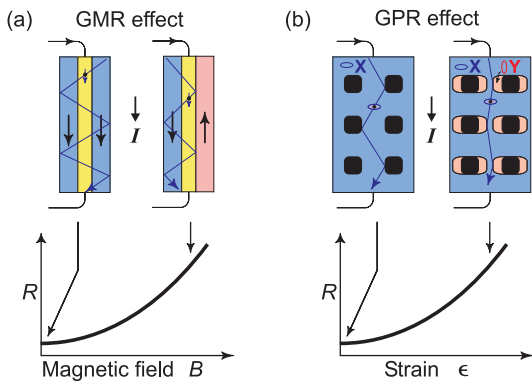


FIG. 4: (Color online) Comparison between: (a) the GMR effect in a layered magnetic metal sandwich structure and (b) the GPR effect in AIAs 2DES with an AD lattice.

We hypothesize that the subharmonic peaks observed in Fig. 3 data arise from an effective narrowing of the “emitter and collector openings” and an elongation of the effective AD boundary for the X -valley electrons upon the application of strain as shown in Fig. 3(d) inset. This is clearly suggested by the simulations of Fig. 2 where the X -valley electrons are excluded near the lower and upper boundaries of the ADs (box A) because of the larger local strain. Several features of Fig. 3 data support this hypothesis: (1) As shown in Figs. 3(c) and (d) all the peak positions are consistent with the orbit diameters being proportional to a/i . (2) The sub-harmonic peaks are pronounced only when strain is applied: Their amplitudes are indeed small near zero strain, increase with ϵ , and then saturate. (3) The AD region with the largest period (i.e. the $1\ \mu\text{m}$ -AD) has the most sub-harmonic peaks; this is consistent with the longer AD boundary allowing more bounces in the electron trajectories.

To further test our conjecture, we performed numerical simulations similar to those used in Ref. [15] but with a variable channel width w to simulate the strain-induced channel-pinching effect [18]. The results, presented in Fig. 3(d), verify our conjecture that a smaller w indeed gives rise to a second sub-harmonic peak that grows in amplitude relative to the fundamental peak. Note also that, as might be expected, Fig. 3(d) simulations show an overall increase in resistance at $B = 0$ for narrower channels, consistent with the PR data of Fig. 1.

Our experimental data and the numerical simulations combined strongly suggest a “channel-pinching effect” in the strained AD lattice for the X -valley electrons. Such an effect explains the emergence of the sub-harmonic commensurability peaks in the magnetoresistance and also the zero-field PR. However, our model leaves an important question unanswered: What is the role of the Y -valley electrons which in fact become the majority carriers and dominate the transport in the blank region with increasing ϵ (lower trace in Fig. 1)? It is likely that the non-uniform strain in the AD region creates a

strong modulating potential, limiting the conductivity of the Y -valley electrons. An increase of resistance with the increase of potential modulation amplitude is indeed common in commensurability oscillation experiments on surface grating devices [19]. It is conceivable that although Y -valley electrons are favored at high strains, their contribution to the overall AD lattice conductivity is suppressed by the strongly modulated potential.

The above channel-pinching picture suggests a remarkable resemblance between our GPR effect and the GMR effect, observed in thin-film structures composed of alternating layers of ferromagnetic and non-magnetic materials [2, 20]. A comparison of these two effects is schematically illustrated in Fig. 4. In each structure, the reversal of polarization of the magnetization (spin) or valley in the regions adjacent to the active channel due to either external magnetic field (B) or applied strain (ϵ) leads to a narrower effective channel width (extra confinement) and possibly additional scattering (for both X and Y -valley electrons) both of which lead to higher resistance.

Regardless of its origin, the GPR exhibited by our AD lattices reveals the extreme sensitivity of their resistance to strain. The data of the $1\ \mu\text{m}$ AD lattice, e.g., yield a maximum strain gauge factor, κ , defined as the fractional change in sample resistance divided by the fractional change in sample length, of over 20,000. This is by far larger than $\kappa \simeq 2$ of standard, metal foil gauges, and is among the largest κ reported for any solid state material. Our structure may find use as an extremely sensitive, low-temperature PR strain sensor to detect ultrasmall forces and distances. Using a simple resistance measurement, we were able to detect strains down to 2×10^{-8} with our samples [21]. Given that the spacing between our Hall bar resistance contacts is $40\ \mu\text{m}$, this strain translates to a displacement of $8 \times 10^{-4}\ \text{nm}$ (about $1/50$ of the Bohr radius)! This sensitivity could be further improved by designing AD lattices with optimized shapes and sizes, and using more sophisticated techniques to measure resistance changes.

We thank the ARO and NSF for support, and K. Vakili for illuminating discussions.

-
- [1] M. N. Baibich *et al.*, Phys. Rev. Lett. **61**, 2472 (1988).
 - [2] G. A. Prinz, Science **282**, 1660 (1998).
 - [3] S. A. Wolf *et al.*, Science **294**, 1488 (2001).
 - [4] C. S. Smith, Phys. Rev. **94**, 42 (1954).
 - [5] Y. P. Shkolnikov *et al.*, Appl. Phys. Lett. **85**, 3766 (2004).
 - [6] O. Gunawan *et al.*, Phys. Rev. Lett. **97**, 186404 (2006).
 - [7] O. Gunawan *et al.*, Nat. Phys. **3**, 388 (2007).
 - [8] O. Gunawan *et al.*, Phys. Rev. B **74**, 155436 (2006).
 - [9] A. Rycerz *et al.*, Nat. Phys. **3**, 172 (2006).
 - [10] E. P. De Poortere *et al.*, Appl. Phys. Lett. **80**, 1583 (2002).
 - [11] M. Shayegan *et al.*, Phys. Stat. Sol. (b) **243**, 3629 (2006).
 - [12] M. Shayegan *et al.*, Appl. Phys. Lett. **83**, 5235 (2003).

- [13] See, e.g., D. Roylance, *Mechanics of Materials* (Wiley, New York, 1995) p. 186.
- [14] D. Weiss *et al.*, Phys. Rev. Lett. **66**, 2790 (1991).
- [15] O. Gunawan *et al.*, Phys. Rev. B **75**, 81304(R) (2007).
- [16] H. van Houten *et al.*, Phys. Rev. B **39**, 8556 (1989).
- [17] F. Nihey *et al.*, Appl. Phys. Lett. **57**, 1218 (1990).
- [18] For simplicity and also because the drawn shape of each AD was intended to be a square, in the simulations of Fig. 3(d) we used square and rectangular shapes for the ADs as indicated in the figure. We repeated the simulations with circular and elliptical AD shapes and obtained qualitatively similar results.
- [19] P. H. Beton *et al.*, Phys. Rev. B **42**, 9229 (1990).
- [20] W. F. Egelhoff *et al.*, J. Vac. Sci. Tech. B **17**, 1702 (1999).
- [21] O. Gunawan, Ph.D. thesis, Princeton University (2007).